



## Research Article

## Learning-based robot assembly method for peg insertion tasks on inclined hole using time-series force information

Zhifei Shen<sup>a,1</sup>, Zhiyong Jiang<sup>b,1</sup>, Jingwang Zhang<sup>c</sup>, Jun Wu<sup>c</sup>, Qiuguo Zhu<sup>a,c,\*</sup><sup>a</sup> Polytechnic Institute, Zhejiang University, Hangzhou 310015, China<sup>b</sup> Robotics Engineering Center, the 21st Research Institute of China Electronics Technology Group Corporation, Shanghai 200233, China<sup>c</sup> Department of Control Science and Engineering, Zhejiang University, Hangzhou 310027, China

## ARTICLE INFO

## Article history:

Received 20 September 2024

Revised 2 December 2024

Accepted 17 December 2024

Available online 5 January 2025

## Keywords:

Manipulator assembly

Peg insertion

Force information

Contact state

Dual-arm

## ABSTRACT

This paper presents a novel method for learning force-aware robot assembly skills, specifically targeting the peg insertion task on inclined hole. For the peg insertion task involving inclined holes, we employ one-dimensional convolutional networks (1DCNN) and gated recurrent units (GRU) to extract features from the time-series force information during the assembly process, thereby identifying different contact states between the peg and the hole. Subsequent to the identification of contact states, corresponding pose adjustments are executed, and overall smooth interaction is ensured through admittance control. The assembly process is dynamically adjusted using a state machine to fine-tune admittance control parameters and seamlessly switch the assembly state. Through the utilization of dual-arm clamping, we conduct key unlocking experiments on bases inclined at varying degrees. Our results demonstrate that the proposed method significantly improves the accuracy and success rate of state recognition compared to previous methods.

© 2025 The Author(s). Published by Elsevier B.V. on behalf of Shandong University. This is an open access article under the CC BY-NC-ND license (<http://creativecommons.org/licenses/by-nc-nd/4.0/>).

## 1. Introduction

In contemporary industrial and academic domains, the peg-in-hole assembly task for industrial robots has garnered substantial attention. The peg-in-hole assembly process involves intricate contact dynamics and is fraught with uncertainties, presenting numerous challenges. Traditional control methods have proven inadequate in meeting the practical requirements of this task [1].

Numerous researchers have tackled peg-in-hole assembly tasks using visual or trajectory-based search methods. Triyonoputro [2] integrated multi-view images with the VGG-16 network to predict the quadrant containing the hole location, thereby expediting the hole search process. Their approach successfully facilitated peg-in-hole assembly experiments on surfaces exhibiting diverse colors and textures. Zakka [3] employed the FCN-ResNet network to formalize the assembly task as a shape matching problem. By acquiring training data through a self-supervised data collection process, they introduced a system named Form2Fit, which achieved a high success rate in assembling objects onto various workpieces under different initial conditions by learning effective

picking and placing strategies. Furthermore, Chhatpar [4] proposed various search trajectories, including connecting discrete points, concentric circles, and spiral paths. Among these, spiral paths are widely utilized for assembling diverse part types, such as square parts [5].

To address the intricacies of peg-in-hole assembly challenges, researchers typically bifurcate peg-in-hole assembly strategies into two distinct modules: a high-level planning module at the upper tier and a low-level control module at the lower stratum [6]. The general low-level control module is typically comprised of the impedance controller or force/position hybrid controller, primarily aimed at resolving compliance control issues. Conversely, the upper layer planning module determines the contact state based on a contact model derived from geometric and environmental constraints, subsequently deducing high-level commands for the lower layer controller, primarily focused on contact state recognition. Jin [7] introduced a contact pose classification method predicated on the contact measurement sequence. They employed a convolutional neural network to classify contact poses using a “first tilt and then rotation” strategy, which was subsequently applied to assembly workpieces with varying geometric shapes. Meanwhile, Yan [8] utilized Support Vector Machines (SVM) to predict the contact state of the base across different inclination angles, integrating force control strategies to ensure secure interaction with the environment.

Several researchers have explored the use of model-free methods to acquire assembly skills from expert demonstrations or

\* Corresponding author.

E-mail address: [qgzhu@zju.edu.cn](mailto:qgzhu@zju.edu.cn) (Q. Zhu).<sup>1</sup> The two authors contributed equally to this work.<sup>2</sup> Given his role as Guest Editor of this journal, Qiuguo Zhu had no involvement in the peer-review of this article and had no access to information regarding its peer-review. The article was handled by Prof. Rui Song.

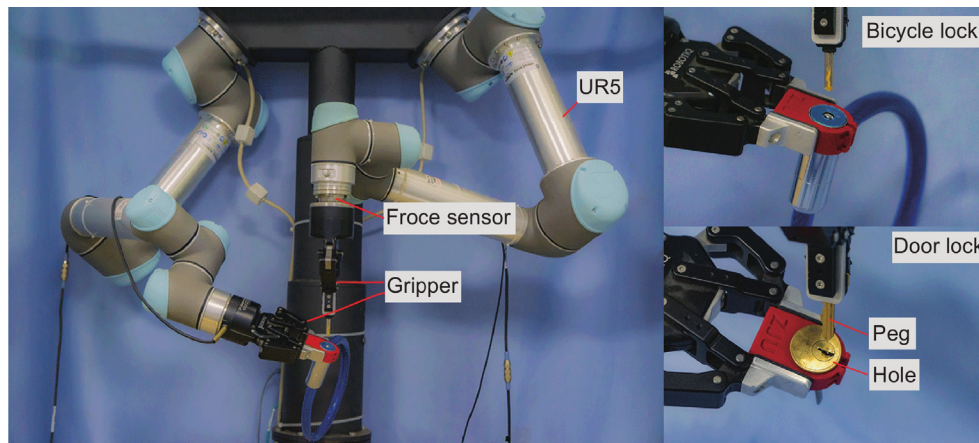


Fig. 1. Peg insertion experimental platform.

environments. Oikawa [9] employed the DQN algorithm to select the stiffness matrix of admittance control, resulting in an accelerated response speed for the assembly task. Meanwhile, Liu [10] introduced an enhanced DMP algorithm to generate motion trajectories. They adopted Cartesian impedance control for trajectory tracking, achieving the simultaneous learning of teaching trajectories and flexible operation skills. Li [11] proposed a skill acquisition method based on DQN, incorporating an SVM classification model as prior knowledge for the reward function. Additionally, Beltran-Hernandez [12] utilized the SAC algorithm to learn the parameters of the parallel force/position hybrid controller for peg-in-hole assembly. They enhanced the training speed through transfer learning technology and domain randomization methods to successfully complete the peg-in-hole assembly task in various stiffness environments.

The advancement of peg-in-hole assembly technology has seen significant progress, with numerous successful applications. However, existing studies predominantly concentrate on control strategies tailored to horizontal hole structures, with limited focus on peg-in-hole assembly strategies for hole structures exhibiting arbitrary tilt angles. After a hole is created at a randomly inclined angle, the data characteristics collected by the force sensor differ from those recorded on a horizontal hole when the peg is in contact with the hole. This variation makes it challenging to accurately identify the different contact states between the peg and the hole while maintaining stable contact in the inclined angle. This paper introduces a novel peg-in-hole assembly strategy designed specifically for arbitrarily inclined holes. The primary contributions of this work are outlined as follows:

- A 1DCNN-GRU contact state recognition model utilizing time-series force data is constructed.
- A novel automated control strategy proposed to address the peg insertion task at arbitrary tilt angles. Unlike previous methods [8], this paper utilizes deep neural networks to automatically extract feature information from temporal forces and identify the contact state between the peg and the hole without the need for manual feature extraction. This improvement enhances the overall automation of the processing flow, resulting in better performance compared to earlier methods. The proposed method has been experimentally applied to two assembly scenarios: door lock and bicycle lock.

The subsequent sections are organized as follows: Section 2 provides a comprehensive problem description pertaining to the research problem addressed in this paper. Section 3 elaborates on the proposed method presented in this paper. Section 4 delineates the specific experimental setup and the corresponding

results obtained. Finally, the conclusion and key findings are summarized in Section 5.

## 2. Problem formulation

In general, the peg-in-hole assembly task can be delineated into two primary stages:

- Search: In this stage, the robot aligns the peg center with the center of the hole. The search stage primarily focuses on locating the target position, specifically the holes that need to be aligned. Its main objective is to address positional errors between the peg and the hole. This is primarily achieved through precise adjustments to the position.
- Insertion: Following the search stage, the robot adjusts the peg's orientation based on the hole's direction and subsequently inserts the peg into the desired position within the hole. The insertion stage primarily addresses the orientation error between the peg and the hole by adjusting the orientation to align them. Simultaneously, adjustments in the depth direction will also be made. Once the target depth is reached, the insertion process is considered complete.

The search phase has been the subject of extensive study. Inoue [13] used a multi-layer LSTM network to estimate Q function, designed action space and reward function in the hole search stage, and completed the assembly task in the search stage. Zou [14] completed the search phase by outputting four types of translation directions in MLP. Compared with the search stage, the insertion stage is more challenging because of complex contact and more uncertainty, which is easy to cause blocking and lead to assembly failure [6]. Therefore, this paper focuses on the insertion phase of the arbitrary tilt angle peg-in-hole assembly task. This paper assumes that the horizontal position error has been eliminated by position control combined with vision. On this basis, the peg insertion task of arbitrary inclined hole is carried out.

## 3. Proposed method

Fig. 2 illustrates the comprehensive method framework of the proposed multi-classification 1DCNN-GRU contact state recognition model, which is based on time-series force information. Unlike previous methodologies [8], the system's input comprises time-series force data collected from a six-dimensional force sensor over a specific duration. Subsequent to gravity compensation and coordinate transformation, this time-series force information is input into the contact state recognition model. The

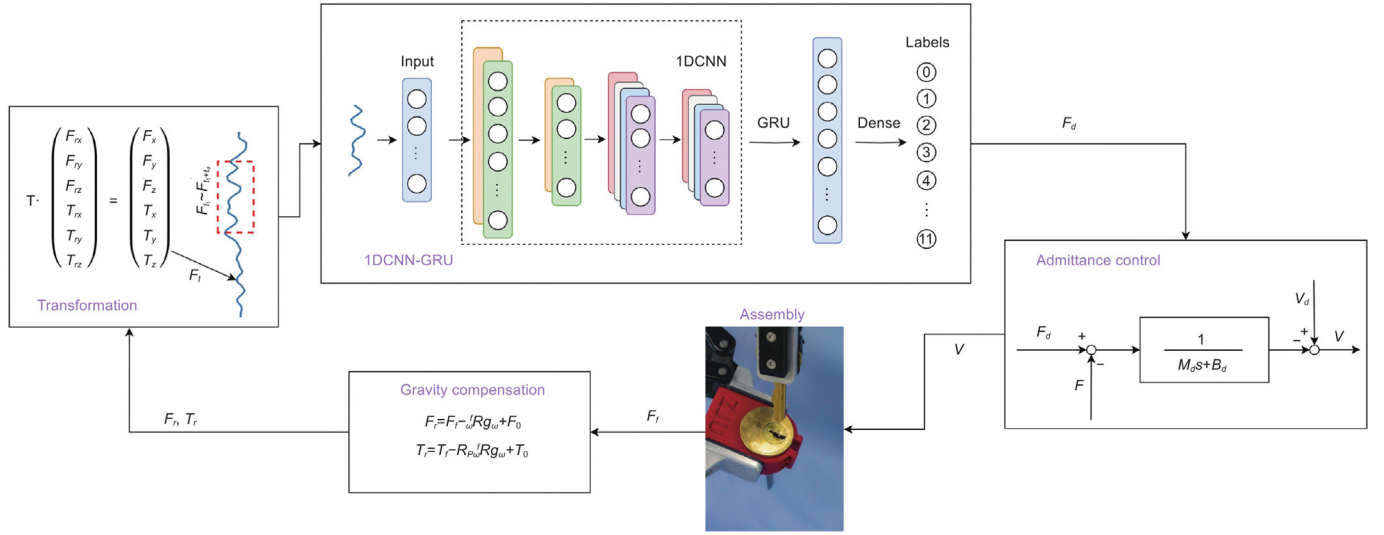


**Fig. 2.** The overall method framework of the proposed multi-classification 1DCNN-GRU contact state recognition model based on the temporal force information.

multi-classification CNN-GRU contact state recognition model then produces admittance control parameters corresponding to the necessary attitude adjustment direction. These parameters are employed to guide the underlying admittance controller, enabling it to regulate the robotic arm's attitude and ensure compliant interaction with the environment.

### 3.1. Gravity compensation

In accordance with Fig. 1, the force data directly obtained by the force sensor is influenced by both the gripper jaws' gravity and the force sensor's zero drift value. To accurately determine the contact force between the gripper's end and the environment, it is essential to compensate for the gravitational impact on the force sensing data. The resultant end contact force data after gravity compensation is represented by

$$F_r = F_f - {}^f_w R g_w + F_0 \quad (1)$$

$$T_r = T_f - R_p {}^f_w R g_w + T_0 \quad (2)$$

where,  $F_r$  and  $T_r$  represent the actual contact force and contact torque between the sensor and the environment, respectively.  $F_f$  represents the original force data measured by the end six-dimensional force sensor, and  $T_f$  indicates the original torque data measured by the same sensor. Additionally,  $F_0$  and  $T_0$  correspond to the sensor's zero force and zero torque data, respectively.  ${}^f_w R$  denotes the rotation matrix from the force sensor coordinate system to the world coordinate system,  $g_w$  signifies the gravity in the world coordinate system, and  $R_p$  is the matrix derived from the position of the gravity center of mass.

## 3.2. 1DCNN-GRU model

### 3.2.1. 1DCNN network

1DCNN, a deep learning model commonly employed for processing time series data, comprises essential components such as a convolutional layer, a pooling layer, and a fully connected layer. The convolutional and pooling layers are designed for potential reuse. Within the convolutional layer, uniform convolutional kernels are utilized to conduct operations on localized input regions along the time-series direction. This approach facilitates the capture of local features and patterns inherent in the time-series data, including signal periodicity, edges, and other distinctive features. Each convolution kernel's convolution with the input

data yields a single frame, allowing the 1DCNN to gain a more profound understanding of the input data's structure. The process of 1D convolution operation is as follows [15]:

$$Y_i^{l+1}(j) = f(K_i^l * X^l(j) + b_i^l) \quad (3)$$

where  $X^l(j)$  denotes the  $j$  local region in the  $l$  layer neural network,  $K_i^l$  is the weight parameter of the  $i$  convolutional kernel in the  $l$ th layer neural network,  $b_i^l$  is the bias parameter of the  $i$ th convolutional kernel in the  $l$  layer neural network,  $*$  denotes the dot-processing operation,  $Y_i^{l+1}(j)$  denotes the  $j$  position of the  $i$  frame in the  $l + 1$  layer neural network, and  $f$  denotes the activation function.

Subsequent to the convolutional layer, the pooling layer typically follows, aiming to diminish the feature map's dimension through downsampling and similar techniques. This process effectively reduces the model's parameter count and enhances its overall robustness. Common pooling operations, such as maximum pooling and average pooling, extract the maximum and average values, respectively, as the resulting values post the pooling operation. Finally, the fully connected layer, typically positioned at the end, serves to transform the feature maps derived from the pooling layer into the model's output, enabling the learning of global features inherent in the input data.

### 3.2.2. GRU network

The Gated Recurrent Unit (GRU) is a type of recurrent neural network primarily designed for processing time series data. Similar to Long Short-Term Memory Networks (LSTM), it addresses challenges such as long-term dependence, gradient vanishing, and gradient explosion, commonly encountered in traditional RNNs. Compared with LSTM, GRU has a smaller number of structural parameters and a simpler overall structure, but it can achieve a comparable perceptual effect, which can largely improve the training efficiency. The forward computation formula for the GRU network is as follows [16]:

$$Z_t = \sigma(W_z X_t + W_z H_{t-1} + B_z) \quad (4)$$

$$R_t = \sigma(W_r X_t + W_r H_{t-1} + B_r) \quad (5)$$

$$\tilde{H}_t = \tanh(W_h X_t + R_t \otimes W_h H_{t-1}) \quad (6)$$

$$H_t = Z_t \otimes H_{t-1} + (1 - Z_t) \otimes \tilde{H}_t \quad (7)$$

where  $X_t$  is the input of time  $t$ ,  $Z_t$  is the update gate of time  $t$ ,  $R_t$  is the reset gate of time  $t$ ,  $\tilde{H}_t$  is the candidate hidden state

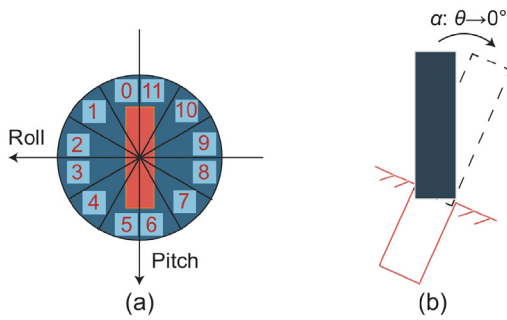


**Fig. 3.** Data acquisition diagram. (a) Top view of hole in 12 classification categories of contact states. (b) A contact state data acquisition side view of 12 classification categories of contact states.

of time  $t$ ,  $H_t$  denotes the hidden state of time  $t$ ,  $H_{t-1}$  denotes the hidden state of time  $t - 1$ , which is the output of the GRU network,  $\sigma$  denotes the sigmoid activation function,  $W$  is the weight parameter of the neural network and  $B$  is the bias parameter of the neural network.

### 3.3. Data acquisition

Illustrated in Fig. 3, the force and torque data from the force-torque sensor are obtained by assessing the angular disparity ( $\alpha$ ) between the peg and the hole, ranging from  $\alpha = \theta$  to  $\alpha = 0$ . The maximum value of  $\alpha$  is 32 degrees. Adjustments to the roll and pitch are made to traverse the hole base at various tilt degrees, enabling the collection of time series force data representing 12 distinct contact states. Subsequently, the acquired force and torque data undergo mean-based filtering. Thereafter, 25 contact force vectors are selected as input for the 1DCNN-GRU model.

### 3.4. Admittance control

To ensure compliant interaction between the manipulator and the environment, this paper employs velocity-based admittance control

$$F_d - F = M_d (\dot{V}_d - \dot{V}) + B_d (V_d - V) \quad (8)$$

where  $V_d$  and  $V$  are the expected velocity and the current actual velocity respectively;  $\dot{V}_d$  and  $\dot{V}$  are the expected acceleration and the current actual acceleration respectively.  $F_d$  and  $F$  are the expected contact force and the current actual contact force.  $M_d$  and  $B_d$  represent the expected inertial parameters and damping parameters of the entire system. When different inertia and damping parameters are configured, the system will exhibit varying inertial and damping characteristics.

The Eq. (8) is discretized and the velocity is differentiated backward

$$V^k = V_d^k - \frac{T (F_d^k - F^k) + M_d (V_d^{k-1} - V^{k-1})}{M_d + T \cdot B_d} \quad (9)$$

where,  $V_d^k$  and  $V^k$  are the expected velocity and the current actual velocity at time  $k$ , respectively.  $V_d^{k-1}$  and  $V^{k-1}$  are the expected velocity and the current actual velocity at time  $k-1$ , respectively.  $F_d^k$  and  $F^k$  are the expected contact force and the current actual contact force at time  $k$ , respectively.  $T$  is the discrete control period. Since the maximum control frequency of UR5 is 125 Hz, the control period  $T = 0.008$  s corresponding to the maximum control frequency is selected in this paper.

Subsequent to acquiring  $V^k$  through velocity-based admittance control, it is directed to the velocity control interface of the manipulator for actual control.

### 3.5. Combine contact state recognition model and admittance control

The entire assembly process is primarily executed through a state machine, transitioning from the current state to the subsequent state upon meeting the designated state switching conditions. The state switching conditions for each state are depicted in Fig. 4.

- $S_1$ : Approach. This state utilizes visual guidance to eliminate the positional error between the peg and the hole, transitioning to the next state when the positional error falls below a predefined threshold. The manipulator employs position control during this phase.
- $S_2$ : Contact. Here, the manipulator's position control shifts to an admittance control method based on velocity. The admittance parameters are configured to facilitate a vertical downward movement until steady contact with the hole is achieved.
- $S_3$ : Align. A contact state recognition model, based on 1DCNN-GRU, is employed to adjust the peg's pose, aligning it with the inclined hole.
- $S_4$ : Fit. As a small part of the peg is inserted into the hole, the admittance control parameters are modified, and torque damping is increased to slow down the pose adjustment process.
- $S_5$ : Insertion. With most of the peg inserted into the hole, the torque damping of the admittance control is further increased, decelerating the attitude adjustment process. Additionally, the expected insertion force is heightened to facilitate continued movement toward the hole.
- $S_6$ : Complete. The peg proceeds to move towards the hole until it is fully inserted into the inclined hole.

## 4. Simulation and experiment

The proposed assembly method was validated using two six-degree-of-freedom Universal Robots (UR5), as depicted in Fig. 1. One UR5 was employed to secure the peg, while another UR5 was utilized to secure the hole base. Communication between the computer and the UR5 controller was facilitated through the TCP/IP protocol within the Robot Operating System. At the end effector of the UR5 industrial robot, two Robotiq 2F-85 grippers were installed to securely hold the parts intended for assembly. Furthermore, the UR5 industrial robot, responsible for gripping the peg, was outfitted with an ATI MINI45 force-torque sensor positioned between the end effector and the gripper. This sensor was instrumental in measuring the six-dimensional contact force during the interaction process. The contact force and contact torque readings were obtained from the ATI NetBox. As shown in Fig. 1, the assembly parts peg and hole include two shapes of door lock and bicycle lock.

This paper validates the peg insertion assembly method through the following sequence. Initially, a comparison of various time series force classification methods is conducted. Subsequently, a state machine is employed to accomplish the peg insertion task. Finally, the efficacy of the proposed method is confirmed through the comprehensive evaluation of the peg-in-hole assembly process.

### 4.1. Contact state recognition model training

A total of 1340 sets of force and torque data were utilized to train 12 categorical contact state recognition models, with 70% of the data allocated for training and 30% for testing. The force and torque sensor's data acquisition frequency is 125 Hz, and

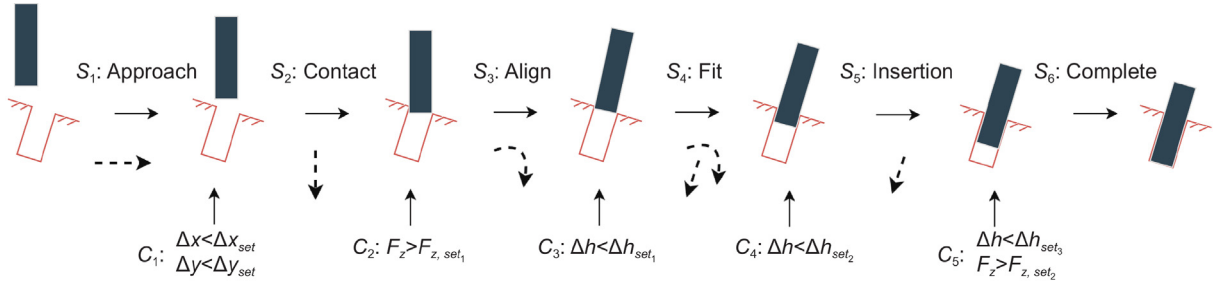


**Fig. 4.** Visualization of overall assembly process based on state machine.  $S_1$  to  $S_6$  represent different states, and  $C_1$  to  $C_5$  represent state switching conditions for each state. The dashed arrow indicates the direction of motion of the peg.  $\Delta x$  is x-axis position error and  $\Delta y$  is y-axis position error.  $\Delta x_{set}$  is x-axis position error threshold and  $\Delta y_{set}$  is y-axis position error threshold.  $\Delta h$  is height error.  $\Delta F_{z,set}$  is z-axis contact force threshold and  $\Delta h_{set}$  is height error threshold.

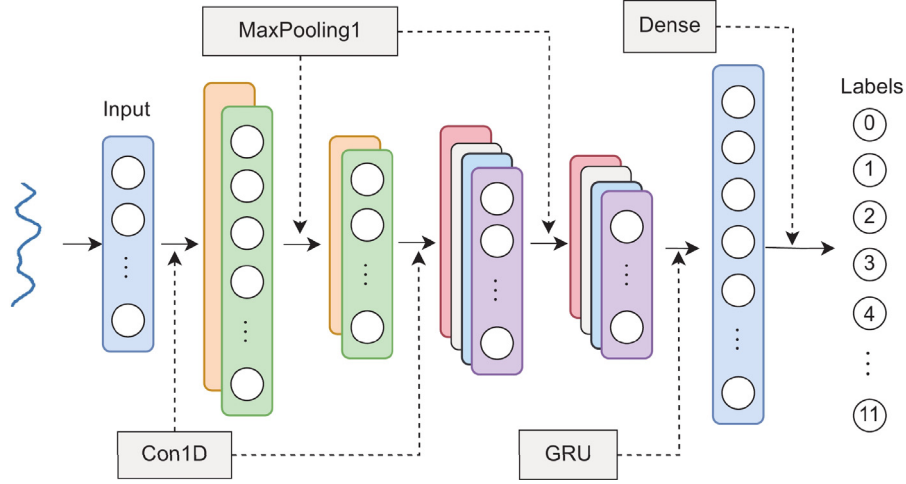


**Fig. 5.** Structure diagram of multi-classification contact state prediction model based on 1DCNN-GRU.

**Table 1**

The parameters of the 1DCNN-GRU.

Layer type	Output shape	Param
Conv1D	(25, 32)	608
MaxPooling1	(13, 32)	0
Conv1D	(13, 64)	6208
MaxPooling1	(7, 64)	0
Dropout	(7, 64)	0
GRU	(128)	74496
Dense	(12)	1548

the input shape  $\in \mathbb{R}^{25 \times 6}$ , corresponding to the force and torque information input within 0.2 s. The comprehensive architecture of the 1DCNN-GRU network is depicted in Fig. 5, while the specific parameters are detailed in Table 1.

To compare the effectiveness of different classification methods, we evaluate 1DCNN, LSTM, GRU, 1DCNN-LSTM, and 1DCNN-GRU. Fig. 6 illustrates the progression of loss and accuracy within the training sets for the various classification methods. The classification outcomes of the test sets using different classification methods are presented in Table 2. It is evident from Table 2 that the classification effectiveness of 1DCNN-GRU on the test set surpasses that of the previously proposed SVM method and also exceeds other deep learning classification methods.

#### 4.2. Insertion process based proposed method

The state machine is utilized for physical verification. The approach (S1) employs position control, while the Contact to Complete phases (S2–S6) utilize admittance control. The settings for admittance control parameters during the assembly

**Table 2**

The classification performance of various methods on the test set.

Method	Loss	Accuracy
SVM	-	94.03%
1DCNN	0.0373	98.26%
LSTM	0.0329	98.51%
GRU	0.0378	98.75%
1DCNN-LSTM	0.0191	99.25%
1DCNN-GRU	<b>0.0174</b>	<b>99.50%</b>

process are presented in Tables 3 and 4. Table 3 illustrates that the multi-classification contact state recognition model based on 1DCNN-GRU was primarily adjusted at Align (S3), Fit (S4), and Insertion (S5). The multi-classification contact state recognition model, based on 1DCNN-GRU, primarily modifies the torque parameters for admittance control, thereby influencing the orientation. Table 4 presents the specific torque parameter settings for different categories. Each group of torque parameters corresponds to a specific attitude adjustment direction, aimed at minimizing the attitude error between the peg and the hole.

In the Contact state (S2), the inertia parameter  $M_d$  is set to  $[50, 50, 80, 0.5, 0.5, 0.5]^T$ , the damping parameter  $B_d$  is set to  $[10^3, 10^3, 10^3, 10, 10, 10]^T$ , and the force parameter  $F_d$  is set to  $[0, 0, 10, 0, 0, 0]^T$ , so that peg moves vertically downward with appropriate inertia and damping until peg contacts the hole. In the Align state (S3), the inertia and damping parameters of the torque are reduced, and the torque parameters are set according to the 1DCNN-GRU contact state recognition model. Transitioning to the Fit state (S4), the inertia and damping parameters of the torque are increased to decelerate the attitude adjustment

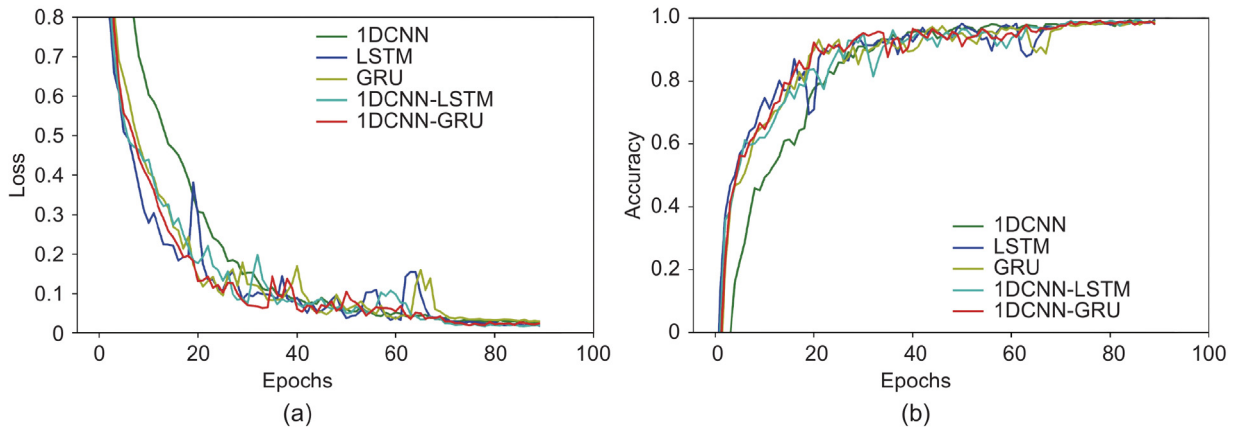


Fig. 6. (a) Loss change process curves of training sets with different classification methods. (b) Accuracy change process curves of training sets with different classification methods.

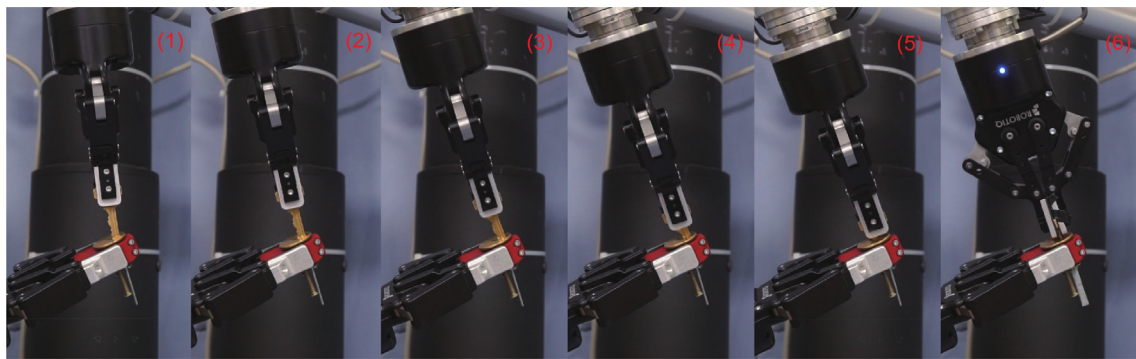


Fig. 7. Snapshots of opening a door lock experiment: (1) make contact with hole; (2), (3) align with 1DCNN-GRU contact state recognition model; (4) fit; (5) insertion; (6) opened lock.

Table 3

The configuration of admittance control parameters during the assembly process.

State	$M_d$	$B_d$	$F_d$
S2	$[50, 50, 80, 0.5, 0.5, 0.5]^T$	$[10^3, 10^3, 10^3, 10, 10, 10]^T$	$[0, 0, 10, 0, 0, 0]^T$
S3	$[50, 50, 50, 0.08, 0.08, 0.5]^T$	$[10^3, 10^3, 10^3, 1.6, 1.6, 10]^T$	$[0, 0, 10, t_{dx}, t_{dy}, 0]^T$
S4	$[50, 50, 50, 0.1, 0.1, 0.5]^T$	$[10^3, 10^3, 10^3, 2, 2, 10]^T$	$[0, 0, 12, t_{dx}, t_{dy}, 0]^T$
S5	$[50, 50, 50, 0.5, 0.5, 0.5]^T$	$[10^3, 10^3, 10^3, 10, 10, 10]^T$	$[0, 0, 20, t_{dx}, t_{dy}, 0]^T$
S6	$[50, 50, 50, 0.5, 0.5, 0.5]^T$	$[10^3, 10^3, 10^3, 10, 10, 10]^T$	$[0, 0, 0, 0, 0, 0]^T$

Table 4

The expected force parameter setting corresponding to the 12 classification categories of contact states.

$F_d$	0	1	2	3	4	5	6	7	8	9	10	11
$t_{dx}$	-0.5	-0.5	-0.1	0.1	0.5	0.5	0.5	0.5	0.1	-0.1	-0.5	-0.5
$t_{dy}$	-0.1	-0.5	-0.5	-0.5	-0.5	-0.1	0.1	0.5	0.5	0.5	0.5	0.1

process, while the expected z-axis force is elevated to 12 N to ensure stable contact between the peg and the hole. Throughout the Insertion state (S5), the inertia and damping parameters of the torque are further increased to slow down the attitude adjustment process, and the expected z-axis force is raised to 20 N to bring the peg and hole into closer contact. Finally, in the Complete state (S6), the force parameter  $F_d$  is set to 0, halting the peg's movement and signifying the completion of the peg insertion process. Snapshots of the experiment are provided in Figs. 7 and 8.

Fig. 9 depicts different stages of lock unlocking assembly process. Figs. 10 and 11 depict the variations in force and position during the peg insertion process. From 0 s to 1 s, in approach state (S1), force/torque are 0 and  $P_z$  slowly decreases. From 1

s to 2.7 s, in contact state (S2),  $F_{dz}$  is set to 10 N.  $F_z$  gradually increases from 0 N to 13 N until the peg and hole are in steady contact ( $p_z^c$  is 0). The change in  $F_z$  at 1.5 s indicates an unstable contact in which the peg slides into the hole. From 2.7 s to 6.2 s, in alignment state (S3), torque damping reduces from 10 to 1.6, and the attitude error is reduced by adjusting the setting value of  $F_d$  according to the 1DCNN-GRU contact state recognition value. From 6.2 s to 8.2 s, in fit state (S4), the force stabilizes around 10 N, and  $p_z^c$  decreases from -2 mm to -7 mm. From 8.2 s to 10.8 s, in insertion state (S5), torque damping increases from 2 to 10 and  $F_{dz}$  is set to 20 N.  $F_z$  increases to 25 N and  $p_z^c$  decreases from -7 mm to -22 mm. From 10.8 s to 12 s, in complete state (S6),  $F_z$  stabilizes at 25 N, while  $p_z^c$  stabilizes at -22 mm.

To evaluate the effectiveness of the proposed method, a dual-arm key unlocking assembly experiment was conducted. In this experiment, the left arm held the lock hole base at an inclined angle ranging from  $-35^\circ$  to  $35^\circ$ , while the right arm held the key for unlocking the assembly. Four different postures were randomly selected, with each posture being tested in 100 trials. The experimental results are presented in Table 5. When compared to the experimental settings in the SVM [8], the assembly success rate using the SVM method decreased from 98.3% to 84% due to

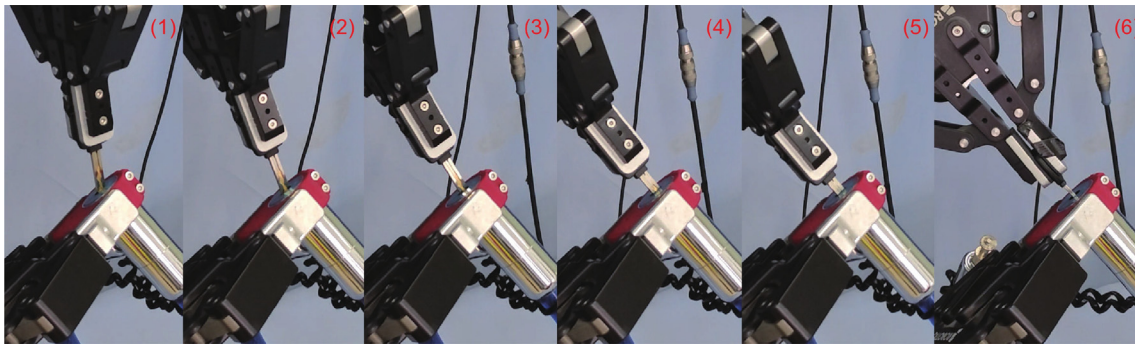


**Fig. 8.** Snapshots of opening a bicycle lock experiment: (1) make contact with hole; (2), (3) align with 1DCNN-GRU contact state recognition model; (4) fit; (5) insertion; (6) opened lock.

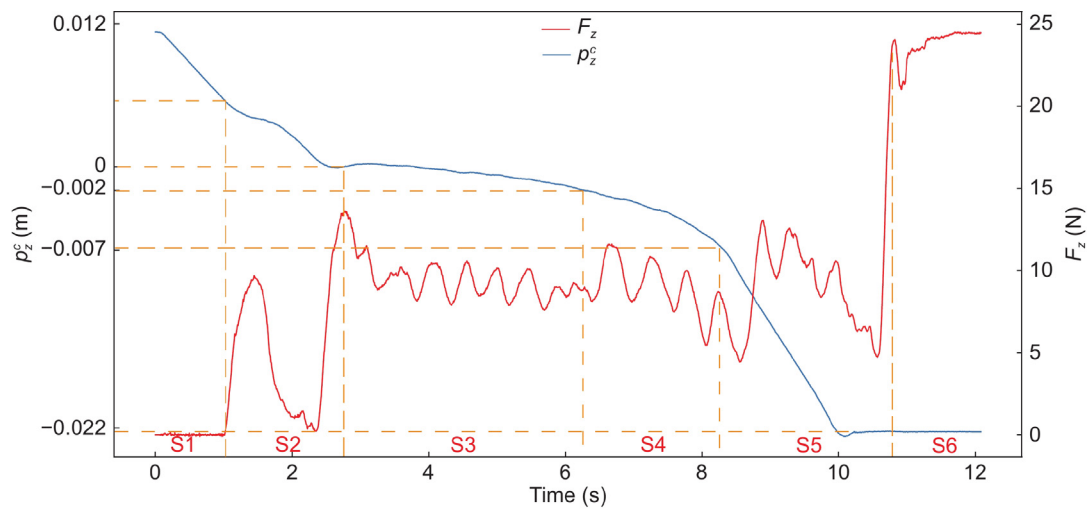


**Fig. 9.** Different stages of lock unlocking assembly process,  $p_z^c$  represents z-axis position with respect to the contact point of the peg and the hole: (S1) Approach (0-1 s); (S2) Contact(1.0-2.7 s); (S3) Align(2.7-6.2 s); (S4) Fit (6.2-8.2 s); (S5) Insertion (8.2-10.8 s); (S6) Complete (10.8-12.0 s).

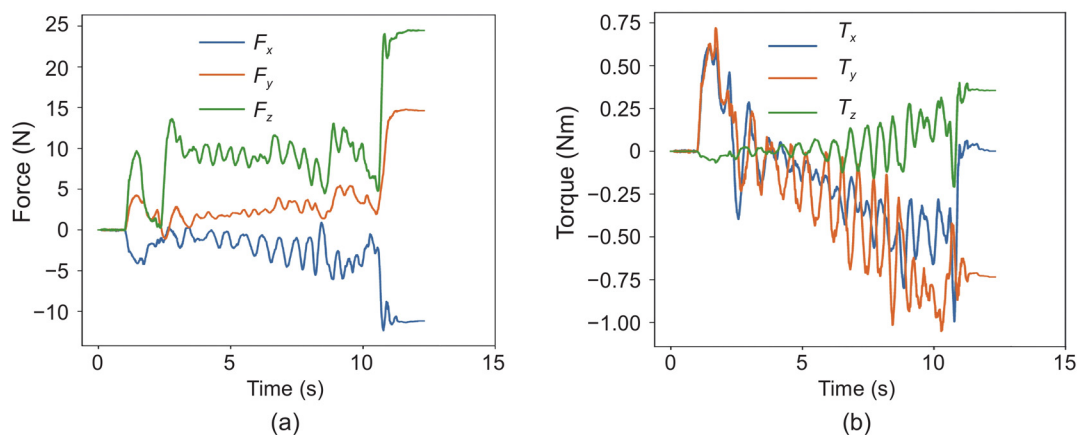


**Fig. 10.** (a) Force data of lock unlocking assembly process. (b) Torque data of lock unlocking assembly process.

the increased tilt angle, which made the task more challenging. The results demonstrate that the 1DCNN-GRU-based method can accomplish the inclined hole assembly task with an experimental success rate of up to 94%, surpassing the previously proposed SVM method (84%).

### 5. Conclusions

This study introduces a novel approach that combines learning and force control to enable robots to acquire assembly skills for tasks involving randomly inclined holes. The method comprises

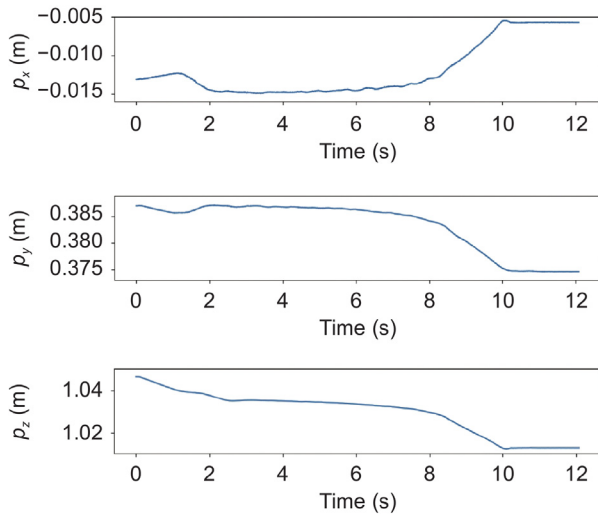


Fig. 11. Position data of lock unlocking assembly process.

Table 5

Comparison of assembly success rate of 400 peg-in-hole experiments between the two methods.

Case	Pose uncertainty ( $\alpha, \beta$ in $^\circ$ )	Success rate (SVM)	Success rate (1DCNN-GRU)
1	(-25, -17)	86%	94%
2	(-18, 30)	81%	92%
3	(23, -20)	90%	100%
4	(25, 8)	79%	90%
Average	-	<b>84%</b>	<b>94%</b>

two primary components. The first component involves a 1DCNN-GRU model, utilized for identifying the contact state, receiving input timing force information, and generating output force control adjustment parameters. The second component integrates a state machine model based on admittance control, responsible for automatic assembly state switching and attitude adjustments based on the force control adjustment parameters produced by the 1DCNN-GRU model. The effectiveness of the proposed method is empirically validated through two distinct scenarios: door lock and bicycle lock. Furthermore, various classification methods are compared to provide insight into the rationale for selecting the 1DCNN-GRU model. The results demonstrate that the proposed method achieves safe and smooth peg insertion, with a maximum assembly success rate of 94%. This significant improvement underscores its potential to enhance the safety and efficiency of peg-in-hole assembly tasks.

#### CRediT authorship contribution statement

**Zhifei Shen:** Methodology, Writing – original draft. **Zhiyong Jiang:** Methodology, Writing – original draft. **Jingwang Zhang:** Investigation, Software. **Jun Wu:** Project administration. **Qiuguo Zhu:** Supervision, Funding acquisition, Conceptualization.

#### Declaration of competing interest

The authors declare that they have no known competing financial interests or personal relationships that could have appeared to influence the work reported in this paper.

#### Acknowledgments

This work was supported by the National Key R&D Program of China (2022YFB4701502), the “Leading Goose” R&D Program of Zhejiang (2023C01177), the 2035 Key Technological Innovation Program of Ningbo City (2024Z300).

#### Appendix A. Supplementary data

Supplementary material related to this article can be found online at <https://doi.org/10.1016/j.birob.2024.100209>.

#### References

- [1] J. Jiang, Z. Huang, Z. Bi, X. Ma, G. Yu, State-of-the-art control strategies for robotic PiH assembly, *Robot. Comput.-Integr. Manuf.* 65 (2020) 101894.
- [2] J.C. Triyonoputro, W. Wan, K. Harada, Quickly inserting pegs into uncertain holes using multi-view images and deep network trained on synthetic data, in: 2019 IEEE/RSJ International Conference on Intelligent Robots and Systems (IROS), IEEE, 2019, pp. 5792–5799.
- [3] K. Zakka, A. Zeng, J. Lee, S. Song, Form2fit: Learning shape priors for generalizable assembly from disassembly, in: 2020 IEEE International Conference on Robotics and Automation (ICRA), IEEE, 2020, pp. 9404–9410.
- [4] S.R. Chhatpar, M.S. Branicky, Search strategies for peg-in-hole assemblies with position uncertainty, in: Proceedings 2001 IEEE/RSJ International Conference on Intelligent Robots and Systems. Expanding the Societal Role of Robotics in the the Next Millennium (Cat. No. 01CH37180), vol. 3, IEEE, 2001, pp. 1465–1470.
- [5] H. Park, J.-H. Bae, J.-H. Park, M.-H. Baeg, J. Park, Intuitive peg-in-hole assembly strategy with a compliant manipulator, in: IEEE ISR, IEEE, 2013, pp. 1–5.
- [6] J. Xu, Z. Hou, Z. Liu, H. Qiao, Compare contact model-based control and contact model-free learning: A survey of robotic peg-in-hole assembly strategies, 2019, arXiv preprint arXiv:1904.05240.
- [7] S. Jin, X. Zhu, C. Wang, M. Tomizuka, Contact pose identification for peg-in-hole assembly under uncertainties, in: 2021 American Control Conference (ACC), IEEE, 2021, pp. 48–53.
- [8] C. Yan, J. Wu, Q. Zhu, Learning-based contact status recognition for peg-in-hole assembly, in: 2021 IEEE/RSJ International Conference on Intelligent Robots and Systems (IROS), IEEE, 2021, pp. 6003–6009.
- [9] M. Oikawa, T. Kusakabe, K. Kutsuzawa, S. Sakaino, T. Tsuji, Reinforcement learning for robotic assembly using non-diagonal stiffness matrix, *IEEE Robot. Autom. Lett.* 6 (2) (2021) 2737–2744.
- [10] N. Liu, X. Zhou, Z. Liu, H. Wang, L. Cui, Learning peg-in-hole assembly using cartesian DMPs with feedback mechanism, *Assem. Autom.* 40 (6) (2020) 895–904.
- [11] F. Li, Q. Jiang, S. Zhang, M. Wei, R. Song, Robot skill acquisition in assembly process using deep reinforcement learning, *Neurocomputing* 345 (2019) 92–102.
- [12] C.C. Beltran-Hernandez, D. Petit, I.G. Ramirez-Alpizar, K. Harada, Variable compliance control for robotic peg-in-hole assembly: A deep-reinforcement-learning approach, *Appl. Sci.* 10 (19) (2020) 6923.
- [13] T. Inoue, G. De Magistris, A. Munawar, T. Yokoya, R. Tachibana, Deep reinforcement learning for high precision assembly tasks, in: 2017 IEEE/RSJ International Conference on Intelligent Robots and Systems (IROS), IEEE, 2017, pp. 819–825.
- [14] P. Zou, Q. Zhu, J. Wu, R. Xiong, Learning-based optimization algorithms combining force control strategies for peg-in-hole assembly, in: 2020 IEEE/RSJ International Conference on Intelligent Robots and Systems (IROS), IEEE, 2020, pp. 7403–7410.
- [15] W. Zhang, G. Peng, C. Li, Y. Chen, Z. Zhang, A new deep learning model for fault diagnosis with good anti-noise and domain adaptation ability on raw vibration signals, *Sensors* 17 (2) (2017) 425.
- [16] J. Chung, C. Gulcehre, K. Cho, Y. Bengio, Empirical evaluation of gated recurrent neural networks on sequence modeling, 2014, arXiv preprint arXiv:1412.3555.